(Au@Ag)@Au double shell nanoparticles loaded on rutile TiO2 for photocatalytic decomposition of 2-propanol under visible light irradiation

doi: info:doi/10.1016/j.apcatb.2015.06.037

(Au@Ag)@Au Double Shell Nanoparticles loaded on Rutile TiO_2 for Photocatalytic Decomposition of 2-Propanol under Visible Light Irradiation

Sunao Kamimura,[1] Takeshi Miyazaki,[1] Ming Zhang,[2] Yuqing Li,[2] Toshiki Tsubota,[1] and Teruhisa Ohno[1*]

[1]*Department of Applied Chemistry, Faculty of Engineering, Kyushu Institute of Technology, 1-1 Sensuicho, Tobata, Kitakyushu 804-8550, Japan*

[2]*School of Chemistry and Chemical Engineering, Yangzhou University, 225002 Yangzhou, China*

ABSTRACT

We synthesized (core@shell)@shell ((Au@Ag)@Au) nanoparticles (NPs) by a multistep citrate reduction method for utilizing photosensitizer of TiO_2. The (Au@Ag)@Au NPs exhibited strong photoabsorption in visible light response due to LSPR excitation of Ag shell, and its LSPR characteristics was stable under long-time visible light irradiation because oxidation of Ag shell was prevented by outermost Au shell. Furthermore, we have successfully loaded (Au@Ag)@Au NPs on rutile TiO_2 by impregnation method. The (Au@Ag)@Au/TiO_2 can oxidize 2-propanol into acetone and CO_2 under visible light irradiation (λ> 440 nm) and its acetone evolution rate was approximately 15 times higher than that of Au/TiO_2. From a result of the comparison between action spectra for acetone evolution and Kubelka-Munk function, it confirmed that photocatalytic activity of (Au@Ag)@Au/TiO_2 was induced by photoabsorption based on LSPR excitation of Ag shell. In addition, photoelectrochemical measurements revealed that electron injection from LSPR excited (Au@Ag)@Au NPs into TiO_2 under visible light irradiation. We proposed the photocatalytic reaction process of (Au@Ag)@Au/TiO_2, in conjunction with optical, structural and photoelectrochemical properties.

Keywords: Photocatalyst, titanium oxide, visible-light response photocatalyst, localized surface plasmon resonance, nanoparticle

1. INTRODUCTION

Since the discovery of photoelectrochemical splitting of water on titanium dioxide (TiO_2) electrodes,[1] the TiO_2 has been intensively studied for its photocatalytic activity, which could be used to convert light energy to storable chemical fuels, or to address environmental issues such as the treatment of waste water and cleaning of exterior windows by degradation of organic molecules.[2-5] The TiO_2 displays photocatalytic activity only when irradiated by ultraviolet (UV) light because of its large band gap (~3.0 eV for rutile and 3.2 eV for anatase).[6] Solar irradiance spectrum contains approximately 4% UV light, whereas visible light comprises 50% and infrared light comprises the remaining 46%. Therefore, the development of visible-light response TiO_2 is strongly demanded for expanding applications utilized solar light as well as fluorescent lamp, incandescent lamp and light-emitting diodes.

So far, many approaches to develop the visible-light response TiO_2 have been proposed, such as chemical doping and photosensitization.[7-10] Chemical doping is most common approach to narrowing bandgap of TiO_2, while doped-ions in the TiO_2 act as recombination centers for photo-excited electrons and holes, resulting in a decrease of photocatalytic activity.[11] Photosensitization of TiO_2 with organic dyes still presents major limitations for applications as photocatalyst because of its the poor stability of the dye, which can undergo desorption, photolysis and oxidative degradation, and fast back electron transfer, which results in low quantum yield for the photocatalytic reaction.[12,13] As an alternative to organic dyes, metallic nanoparticles (NPs) have been successfully used as photosensitizers for the TiO_2 due to its stability and strong photoabsorption at visible light based on localized surface plasmon resonance (LSPR). Here the LSPR is coherent oscillation of electrons at surface of the metallic NPs upon incident light

irradiation.[14] The LSPR-induced photocatalytic activity of TiO_2 was first described by Tatsuma *et al.* in 2005 in a study where they found that gold (Au) NPs loaded a TiO_2 (Au/TiO_2) films can photocatalytically oxidize ethanol and methanol at the expense of oxygen reduction under visible light.[15] Kowalska *et al.* further investigated the photocatalytic decomposition of 2-propanol by utilizing Au/TiO_2 powders, and they proposed the LSPR-induced photocatalytic reaction process: (1) Incident photons are absorbed by the Au NPs through its LSPR excitation, (2) electrons in the Au NPs are injected into the conduction band of TiO_2, and (3) the resultant electron-deficient Au NPs could oxidize 2-propanol to be recovered to the original metallic Au NPs state.[15] To date, there are many reports concerning the photocatalytic activity of Au/TiO_2 and its mechanism.[16-19]

The silver (Ag) NPs also display strong photoabsorption in the visible range based on LSPR, and Ag/TiO_2 shows a higher incident-photon-to-current efficiency than that of Au/TiO_2 under irradiation of visible light.[20] However, Ag NPs possess severe susceptibility to oxidation; that is, Ag NPs were oxidized at the interface between Ag and TiO_2, which leads to form silver oxide.[21] The oxidation of Ag gives rise to a decrease in the photoabsorption intensity and a shift in the LSPR wavelength.[22,23] Therefore, if oxidation of Ag NPs on the TiO_2 can be prevented, it is expected to gain and keep a high photocatalytic activity under visible light irradiation. The present research has carried out from this stand point. Our attention is now toward the (core@shell)@shell structure, (Au@Ag)@Au NPs, where core Au and outermost Au shell provide electrons to Ag shell for prevent of the Ag oxidation.[24] This double shell structure (Au@Ag)@Au NPs were first revealed by Maenosono *et al.* for use as probes in sensing and bio-diagnostics applications, and they revealed that (Au@Ag)@Au NPs

exhibited photoabsorption in the visible range based on LSPR of middle Ag shell.[25] However, the photocatalytic activity of (Au@Ag)@Au double shell NPs loaded on TiO_2 is still not understood.

We synthesized (core@shell)@shell (Au@Ag)@Au NPs by a multistep citrate reduction method for utilizing as photosensitizer of TiO_2, and successfully loaded on rutile TiO_2 by impregnation method. The (Au@Ag)@Au/TiO_2 exhibited photocatalytic activity for decomposition of 2-propanol under visible light irradiation (λ >440 nm), and its photocatalytic reaction rate was approximately 15 times higher than that of Au/TiO_2. In this paper, we present the photoctalytic activity of (Au@Ag)@Au/TiO_2 and discuss its photocatalytic reaction process in conjunction with optical, structural and photoelectrochemical properties.

2. EXPERIMENTAL SECTION

2.1. Preparation of (Au@Ag)@Au NPs and rutile TiO_2

The (Au@Ag)@Au NPs were synthesized by a multistep citrate reduction method as follows (refer Scheme 1). First, Au NPs were prepared which used as seeds for the synthesis of (Au@Ag)@Au NPs. The hydrogen tetrachloroaurate (III) tetrahydrate (99.0%, Wako Pure Chemical Industries. Ltd.), trisodium citrate (99.0%, Wako Pure Chemical Industries. Ltd.) and polyvinylpyrrolidone ($(C_6H_9NO)_n$; n=27~32 Wako Pure Chemical Industries. Ltd.) as starting reagents were mixed together thoroughly in distilled water at 70 °C. The mixed solution was stirred for 1 h and cooled to room temperature. The obtained Au NPs suspension was a dark reddish colour with a LSPR band at 522 nm, and average diameter of Au NPs was 9 nm (Supporting information Fig. S1). Next, Ag shell was grown on the Au seeds via seed-mediated growth for

(core@shell) Au@Ag NPs. The obtained Au NPs suspension was heated to reflux, then silver nitrate (99.5%, Wako Pure Chemical Industries. Ltd.) and the trisodium citrate were simultaneously added. After refluxing for 30 minutes, outermost Au shell was grown on the Au@Ag NPs by adding the hydrogen tetrachloroaurate (III) tetrahydrate and the trisodium citrate solution. The mixed solution was reflexed for 30 minutes and cooled to room temperature. Then (Au@Ag)@Au NPs were obtained.

The rutile TiO_2 crystals were synthesized by hydrothermal method, which our previously reported.[26] In the synthesis procedure, a chemical solution was put in a sealed Teflon-lined autoclave reactor containing 50 ml aqueous solution of titanium trichloride, sodium chloride and poly(vinyl pyrrolidone). The solutions were then put into a 180 °C oven for 10 h. The substrate was centrifuged and rinsed with deionized water and then dried in a vacuum oven. After hydrothermal treatment, the organic compounds that remained or were adsorbed on the surface of TiO_2 particles were removed by ultraviolet (UV) irradiation with a 500-W super-high-pressure mercury lamp (Ushio, SX-UI501UO) for 24 h. The particles were dried under reduced pressure at 60 °C for 6 h. Then rutile TiO_2 crystals were obtained.

2.2. Loading (Au@Ag)@Au NPs on rutile TiO_2

The (Au@Ag)@Au NPs were loaded on rutile TiO_2 by impregnation method. The impregnation was carried out by the following procedures: firstly, UV light (λ=365 nm, intensity; 3 mW/cm^2) was irradiated to rutile TiO_2 for 3 days to remove organic compounds that remained or were adsorbed on the surface of TiO_2. Next, rutile TiO_2 powder and colloidal (Au@Ag)@Au NPs were put into an egg-plant shaped flask. This mixed-solution was dispersed by sonication for 10 minutes and then dried by using

a rotary evaporator on a water bath. After evaporation, the residue was washed with distilled water several times. Finally, the residual water was completely removed by using vacuum freeze drying method. Then (Au@Ag)@Au/ TiO_2 were obtained. The Au@Ag NPs and Au NPs were also loaded on rutile TiO_2 by impregnation method, which was same procedure mentioned above. It should be noted that amount of loading (Au@Ag)@Au NPs, Au@Ag NPs and Au NPs on TiO_2 were optimized at 0.75wt% (Supporting information Fig. S2).

2.3. Characterization

The (Au@Ag)@Au NPs were characterized by field emission high resolution transmission electron microscope (HR-TEM; Tecnai G2 F30 S-TWIN, FEI) with a high-angle annular dark-field (STEM-HAADF) detector, energy-dispersive X-ray spectroscopy (EDS) elemental mapping. Absorption spectrum of colloidal (Au@Ag)@Au NPs acquired at room temperature with a UV/VIS spectrometer (UV-2600, Shimadzu Co.). The crystalline phase of rutile TiO_2 was characterized by using a powder X-ray diffraction (XRD) instrument (MiniFlex II, Rigaku Co.) with CuKα (λ=1.5418 Å) radiation (cathode voltage: 30 kV, current: 15 mA). The diffuse reflectance spectrum acquired at room temperature with a UV/VIS spectrometer (UV-2600, Shimadzu Co.) attached to an integral sphere. X-ray photoelectron spectroscopy (XPS) measurements were performed using a Kratos AXIS Nova spectrometer (Shimazu Co.) with a monochromatic Al Kα X-ray source. The binding energy was calibrated by taking the carbon (C) 1s peak of contaminant carbon as a reference at 248.7 eV.

2.4. Photocatalytic decomposition of 2-propanol

Photocatalytic activity of (Au@Ag)@Au/TiO_2 was evaluated by photocatalytic decomposition of 2-propanol. The sample powders of 0.16 mg were spread on a glass dish (4.0 cm^2) and placed in a Tedlar bag (AS ONE Co. Ltd.) with a volume of 125 cm^3. The Tedlar bag was sealed by laminating after the placement of the glass dish, and then gaseous 2-propanol with 500 ppm was injected into the Tedlar bag, in which gaseous composition in the Tedlar bag was 79% N_2, 21% O_2, <0.1 ppm of CO_2 and 500 ppm of 2-propanol. After 2-propanol had reached absorption equilibrium (after 2 hours), visible light irradiated to sample at room temperature. A 500-W xenon lamp (Ushio, SX-UI501XQ) was used as a light source and the wavelength of photoirradiation was controlled by Yellow-44 filter (λ > 440 nm, Asahi Techno Glass Co.). The intensity of light was adjusted 50 mW/cm^2. The concentrations of 2-propanol, acetone and carbon dioxide (CO_2) were estimated by gas chromatography (Shimadzu, GC-8A, FID detector) with a PEG-20 M 20% Celite 545 packed glass column and by gas chromatography (Shimadzu, GC-9A, FID detector) with a TCP 20% Uniport R packed column and methanizer (GL Sciences, MT-221), respectively.

2.5. Photoelectrochemical measurement

Photoelectrochemical measurement was carried out by using electrochemical analyzer (604D, ALS Co.) with three–electrode system, where the (Au@Ag)@Au/TiO_2 electrode, the platinum, and silver-silver chloride (Ag/AgCl) electrode were used as working electrode, counter electrode, and reference electrode, respectively. The electrolyte was non-bubbled 0.1 M NaOH solution and its potential hydrogen (pH) was pH=14. The light source was used a Xe lamps equipped with yellow-44 cut off filter

(λ > 440 nm, Asahi Techno Glass Co.). The light intensity was determined by utilizing a thermopile power meter (ORION-TH), and the intensity was 50 mW/cm^2. The (Au@Ag)@Au/TiO_2 electrode was fabricated on the fluorine doped tin oxide (FTO) glass as following procedure; firstly, rutile TiO_2 crystal was deposited onto FTO glass in acetone solution by electrophoretic method. After deposition of rutile TiO_2 layer, (Au@Ag)@Au NPs was also deposited onto TiO_2/FTO glass in distilled water by electrophoretic method.

3. RESULTS AND DISCUSSION

3.1. Characterization of (Au@Ag)@Au NPs.

Figure 1 shows a TEM photograph and distribution of colloidal (Au@Ag)@Au NPs, revealing that (Au@Ag)@Au NPs have an average particle size of 18.0 nm within a relatively sharp distribution with standard deviation of 2.8 nm. Figure 2(a) shows a STEM-HAADF image of (Au@Ag)@Au NPs. Since the intensity (brightness) is approximately proportional to the square of the atomic number (Z^2) in STEM-HAADF image, heavier Au atoms (atomic number; Z= 79) give rise to a brighter image than lighter Ag atoms (Z= 47). This image indicates that core Au was covered by Ag shell in (Au@Ag)@Au NPs. To investigate outermost Au shell in (Au@Ag)@Au NPs, EDS elemental mapping was performed. The data acquisition with high resolution was difficult due to sample drift, thereby, we compared EDS elemental mapping between (Au@Ag)@Au NPs and Au@Ag NPs to clarify outermost Au shell. As shown in Fig. 2 (b), (c), (e) and (f), the distribution of Au M edge of Au@Ag NPs was located at only center of particles. On the other hands, the distribution of Au M edge of (Au@Ag)@Au

NPs was spread around of particles, suggesting that outermost Au shell could be formed in (Au@Ag)@Au NPs.

For utilize (Au@Ag)@Au NPs as photosensitizers of TiO_2, it is required visible-light response and stability. We investigated LSPR characteristics of colloidal (Au@Ag)@Au NPs before and after exposure in Xe lamp equipped Y-44 cut-off filter (λ >440 nm). Figure 3 shows absorption spectrum of colloidal (Au@Ag)@Au NPs, together with that of Au@Ag NPs and Au NPs in aqueous solutions. Before exposure in Xe lamp, colloidal (Au@Ag)@Au NPs exhibited strong absorption peaks centered at 420 nm. This peak was considered to be due to the LSPR excitation of Ag. This observation is consistent with a previous report by Maenosono *et al*.[23] After exposure in Xe lamp for 72 hours, absorption spectrum of (Au@Ag)@Au NPs was barely changed, implying that (Au@Ag)@Au NPs was stable at long-time visible light irradiation.

On the other hands, absorption spectrum of Au@Ag NPs changed after exposure in Xe lamp; a LSPR peak (λ_{max}=407 nm) intensity was decreased and additional LSPR peak centered at 650 nm was observed. Similar phenomenon has been reported by Mirkin *et al*. in a study where they found a decrease of LSPR peak intensity of colloidal Ag NPs (λ_{max}=400 nm) with a concomitant increased of LSPR peak intensity at 670 nm under 40-W fluorescent lamp illumination.[27] They revealed that fluorescent lamp irradiation for colloidal Ag NPs led to morphology change, resulting in a change of LSPR characteristics. As shown in Fig. 3, STEM-HAADF and the EDS elemental mapping images indicated that a degradation of absorption spectrum of the Au@Ag must be due to morphology change of Ag shell (see Fig. 3(b)). Wu *et al*. revealed that morphological conversions of Ag NPs were caused by coupling the photo-oxidative dissolution and the subsequent photoreduction of aqueous Ag^+ ions.[28] Therefore, it is

highly possible that Ag shell in Au@Ag NPs were oxidized by visible light irradiation, which leads to morphological conversions, resulting in a decrease of absorption intensity and a change in the absorption spectrum. In contrast, LSPR characteristics of (Au@Ag)@Au NPs was stable under long-time visible light irradiation because oxidation of Ag shell may be prevented by outermost Au shell.

3.2. Characterization of (Au@Ag)@Au NPs/TiO_2.

Figure 4(a) shows a TEM photograph of rutile TiO_2. The rod-like morphology was confirmed and most of rutile rods consisted of flat side surfaces and triangular-like caps, similar to the structure reported for rutile rods with {110} and {111} exposed crystal faces and longer length along the [001] direction.[26,29] Figure 4(b) shows a TEM photograph of rutile TiO_2 with (Au@Ag)@Au NPs. Small (Au@Ag)@Au NPs were observed and average diameter was determined to be ca. 19 nm, indicating that (Au@Ag)@Au NPs were successfully loaded on surface of rutile TiO_2 by impregnation method.

Figure 4(c) shows diffuse reflection spectrum of (Au@Ag)@Au/TiO_2, together with that of bare rutile TiO_2, Au/TiO_2, Au@Ag/TiO_2. The bare rutile TiO_2 exhibited only strong photoabsorption at $\lambda < 400$ nm, which was ascribed to the band-gap excitation. In the case of Au/TiO_2, additional absorption peak was observed at around 560 nm. Kowalska *et al.* reported that photoabsorption of Au NPs loaded on rutile TiO_2 was observed at around 550 nm due to its LSPR excitation. Therefore, photoabsorption observed in Au/TiO_2 was attributed to LSPR excitation of the loaded Au NPs. (Au@Ag)@Au NPs or Au@Ag NPs loaded on rutile TiO_2 exhibited a strong absorption peak centered at 484 nm or 486 nm, respectively. These absorption peaks were ascribed

to LSPR excitation of Ag shell in loaded (Au@Ag)@Au NPs and Au@Ag NPs on the basis of absorption spectrum of colloidal (Au@Ag)@Au NPs and Au@Ag NPs (refer to Fig. 3).

3.3. Photocatalytic activities of (Au@Ag)@Au NPs/TiO_2 for 2-propanol oxidation.

The photocatalytic activity was evaluated by oxidation of 2-propanol in gas phase. Figure 5 shows time course of acetone and CO_2 evolution from decomposition of 2-propanol over (Au@Ag)@Au/TiO_2 under irradiation of Xe lamp equipped with Y-44 cut-off filter (λ> 440 nm, 30 mW/cm^2). Acetone evolution was increased almost linearly with irradiation time up to 6 h, and followed by a gradually decrease with irradiation time due to accumulation of acetone on surface of (Au@Ag)@Au/TiO_2. After prolonged visible light irradiation, the acetone was finally decomposed into CO_2. This behavior is plausible as it is known that 2-propanol decomposes into CO_2, which is final product, via acetone, the intermediary product.[30-32] It should be noted that the acetone and CO_2 were detect neither under dark conditions nor under visible light irradiation in absence of (Au@Ag)@Au/TiO_2.

Action spectrum is strong tool for determining whether a reaction observed in (Au@Ag)@Au/TiO_2 occurs via a photo-induced process or thermocatalytic process. To obtain an action spectrum, acetone evolution from decomposition of 2-propanol over (Au@Ag)@Au/TiO_2 was measured at room temperature under visible light irradiation by using light-emitting diodes peaking at 455 nm, 470 nm, 505 nm, 530 nm, 625 nm and 720 nm, respectively. Apparent quantum efficiency (AQE) at each wavelength was calculated form the ratio of the amount of the acetone and the amount of incident

photons, using the following equation;

$$AQE = \frac{amount\ of\ acetone\ molecules \times 2}{amount\ of\ incident\ photons}$$

As shown in the Fig. 6, the AQE was good agreement with the Kubelka-Munk function of (Au@Ag)@Au/TiO_2, indicating that photocatalytic activity of (Au@Ag)@Au/TiO_2 was induced by photoabsorption based on LSPR excitation of Ag shell. Figure 7 shows the cycle tests of acetone evolution from decomposition of 2-propanol over (Au@Ag)@Au/TiO_2 under irradiation of Xe lamp equipped with Y-44 cut-off filter (λ> 440 nm, 30 mW/cm^2). In the first cycle, acetone evolution was increased almost linearly with irradiation time and followed by gradually decreased with irradiation time, which were discussed above. After 24 h and 48 h irradiation, residual acetone was removed by evacuation and additional 2-propanol was injected and irradiation again. Just the same as with the first cycle, acetone evolution was increased with irradiation time indicating that (Au@Ag)@Au/TiO_2 continuously decomposed 2-propanol under visible light irradiation without losing its activity.

Thus, (Au@Ag)@Au/TiO_2 can oxidize 2-propanol into acetone and CO_2 under visible light irradiation (λ> 440 nm) and its activity was attributed to LSPR excitation of Ag shell. Therefore, we calculated the turnover number of Ag shell in loaded (Au@Ag)@Au NPs. The present sample (0.75 wt% (Au@Ag)@Au/TiO_2) contained ca. 8.8 μmol Ag, and CO_2 evolution was confirmed to be ca. 2.7 μmol after irradiation for 24 h (see Fig. 4). Assuming that six photons are required to produce one CO_2 molecule, as following equations;

$$(CH_3)_2CHOH + 5H_2O + 18h^+ \rightarrow 3CO_2 + 18H^+$$

The turnover number of Ag shell in (Au@Ag)@Au NPs was more than ca. 1.84,

which is enough to prove that a reaction observed was photocatalytic reaction.

Figure 8 shows the comparison of acetone and CO_2 evolution rates of (Au@Ag)@Au/TiO_2, Au@Ag/TiO_2, Au/TiO_2 and bare rutile TiO_2 under Xe lamp irradiation equipped with Y-44 cut-off filter (λ> 440 nm, 30 mW/cm^2). As shown in this figure, acetone and CO_2 evolution rates were increased in the order to bare TiO_2 < Au/TiO_2 << Au@Ag/TiO_2 < (Au@Ag)@Au/TiO_2, implying that LSPR excitation of Ag could produce higher photocatalytic activity than that of Au. Although, acetone evolution rate of Au@Ag/TiO_2 was same as that of (Au@Ag)@Au/TiO_2, the CO_2 evolution rate of Au@Ag/TiO_2 was smaller than that of (Au@Ag)@Au/TiO_2. To clarify this phenomenon, XPS measurement has been done before and after photocatalytic activity tests for decomposition of 2-propanol, and the results of the Ag *3d* spectra are shown in Fig. 9. Before exposure in visible light, both of sample exhibited two sharp peaks at 367.9 eV and 374 eV, which were attributed to typical values of Ag $3d_{5/2}$ and $3d_{3/2}$, respectively. After photoirradiation, Ag *3d* XPS spectrum of Au@Ag/TiO_2 shifted to lower binding energy, which peaked at 367.4 eV and 373.4 eV, respectively. These peaks were identified to be silver oxide AgO,[33] indicating that Au@Ag NPs were oxidized by irradiation of visible light. Previously Sukhishvili *et al.* revealed that oxidation of Ag NPs surface hinders charge transfer between Ag and organic molecules.[34] Therefore, we speculated that oxidation of Au@Ag NPs on the TiO_2 suppress photocatalytic oxidation of acetone under long term photoirradiation, resulting in a lower CO_2 evolution compared with (Au@Ag)@Au/TiO_2.

3.4. Photocatalytic reaction process of (Au@Ag)@Au NPs/TiO_2.

There have been several reports concerning the mechanism of LSPR-induced

photocatalytic reaction of the Au NPs/TiO_2.[14-16] As for the reaction mechanism, electron injection from LSPR excited Au NPs to TiO_2 and subsequent oxidation of 2-propanol at Au NPs have been proposed. Actually, Furube *et al.* observed the electron transfer from excited Au NPs to TiO_2 particles by means of femtosecond transient absorption spectroscopy.[16]

To clarify the electron transfer process of (Au@Ag)@Au/TiO_2, photoelectrochemical measurement has been done. Figure 10 shows linear sweep voltammetry of the (Au@Ag)@Au/TiO_2 electrode in 0.1 M NaOH solutions with irradiation of visible light (λ >440 nm), together with that of rutile TiO_2 electrode. As clearly in this figure, the (Au@Ag)@Au/TiO_2 photoelectrode exhibited an anodic photocurrent in response to irradiation of visible light, and the anodic photocurrent density reached 0.1 $\mu A/cm^2$ at 0 V applied potential versus Ag/AgCl. In contrast, bare rutile TiO_2 electrode did not exhibit an anodic photocurrent under visible light. These results supporting that electron transfer from LSPR excited (Au@Ag)@Au NPs to the rutile TiO_2 has occurred subsequent oxidation of water at (Au@Ag)@Au NPs.

On the basis of above results, we proposed the reaction process for the photocatalytic decomposition of 2-propanol over (Au@Ag)@Au/TiO_2 as follows; (1) When visible light was irradiated to the (Au@Ag)@Au/TiO_2, the photons are absorbed by the middle Ag shell of (Au@Ag)@Au due to LSPR excitation, as was proved by action spectrum analysis. (2) The excited electrons in the middle Ag shell may be injected to the conduction band of rutile TiO_2. Then, electron-deficient Ag shell (Ag^+ state) received electrons from outermost Au shell to be recovered to original Ag state. (3) The resultant electron-deficient Au shell can oxidize organic compounds, such as 2-propanol and acetic acid.

4. CONCLUSIONS

Colloidal (core@shell)@shell (Au@Ag)@Au) NPs were synthesized and successfully loaded on rutile TiO_2 by using an impregnation method. The (Au@Ag)@Au NPs loaded on the TiO_2 showed a strong photoabsorption at around 420 nm due to LSPR of Ag shell, and its LSPR characteristics was stable under long-time visible light irradiation because oxidation of Ag shell was prevented by outermost Au shell. Furthermore, we revealed that (Au@Ag)@Au NPs/TiO_2 can oxidize 2-propanol into acetone and CO_2 under visible light irradiation (λ> 440 nm) and the acetone generation rate of (Au@Ag)@Au NPs/TiO_2 was approximately 15 times higher than that of Au NPs/TiO_2. From a result of the comparison between action spectra for acetone evolution and Kubelka-Munk function, it confirmed that photocatalytic activity of (Au@Ag)@Au/TiO_2 was induced by photoabsorption based on LSPR excitation of Ag shell. The turnover number of Ag shell in (Au@Ag)@Au/TiO_2 more than ca. 1.8, which is enough to prove that a reaction observed was photocatalytic reaction. Photoelectrochemical measurements revealed that electron injection from LSPR excited (Au@Ag)@Au NPs into TiO_2 under visible light irradiation. We proposed the photocatalytic reaction process for (Au@Ag)@Au/TiO_2.

ASSOCIATED CONTENT

Supporting information TEM photograph and size distributions of colloidal Au NPs. Photocatalytic activity of decomposition of 2-propanol into acetone.

This material is available free of charge via the Internet at http://pubs.acs.org.

AUTHOR INFORMATION

Corresponding author tohno@che.kyutech.ac.jp

Acknowledgements

The authors thank to Prof. Tetsuya Haruyama, Prof. Yoichi Shimizu of Kyushu Institute of Technology, and Takeshi Fukuma of Kanazawa Univ. for their valuable contributions to this study. This work was partially supported by a JST ACT-C program and JST PRESTO program.

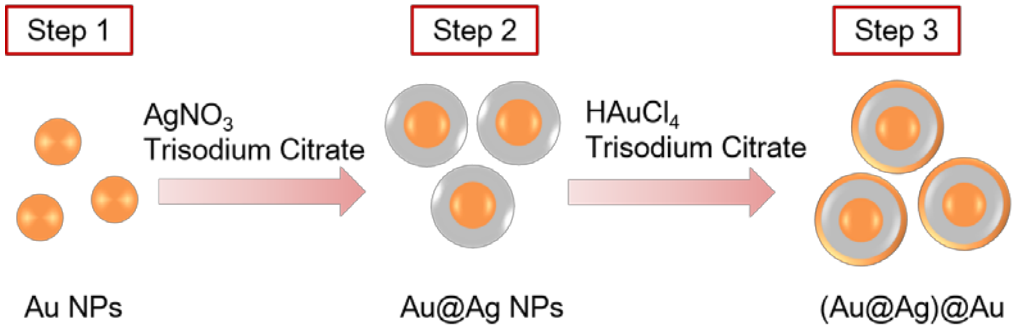

Scheme1. Synthesis procedure for (Au@Ag)Au NPs

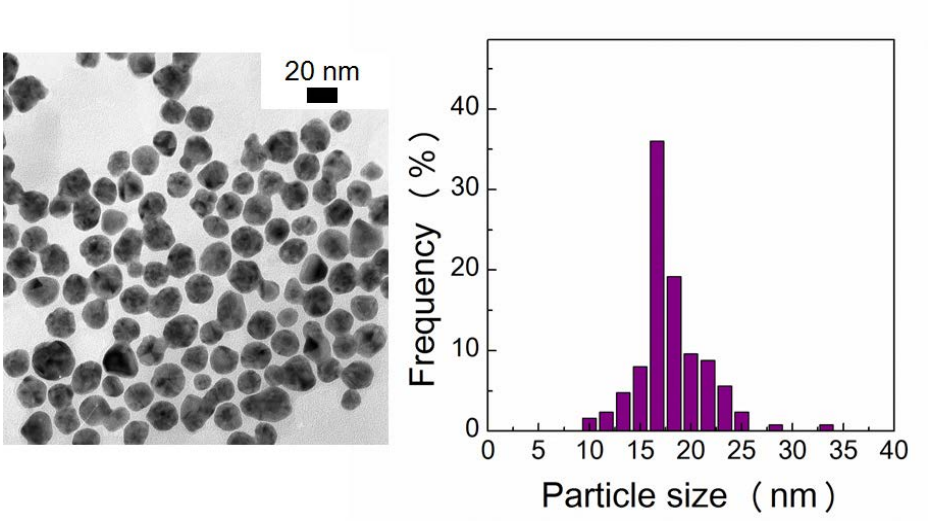

Figure 1. TEM photograph (left) and size distributions (right) of colloidal (Au@Ag)Au NPs.

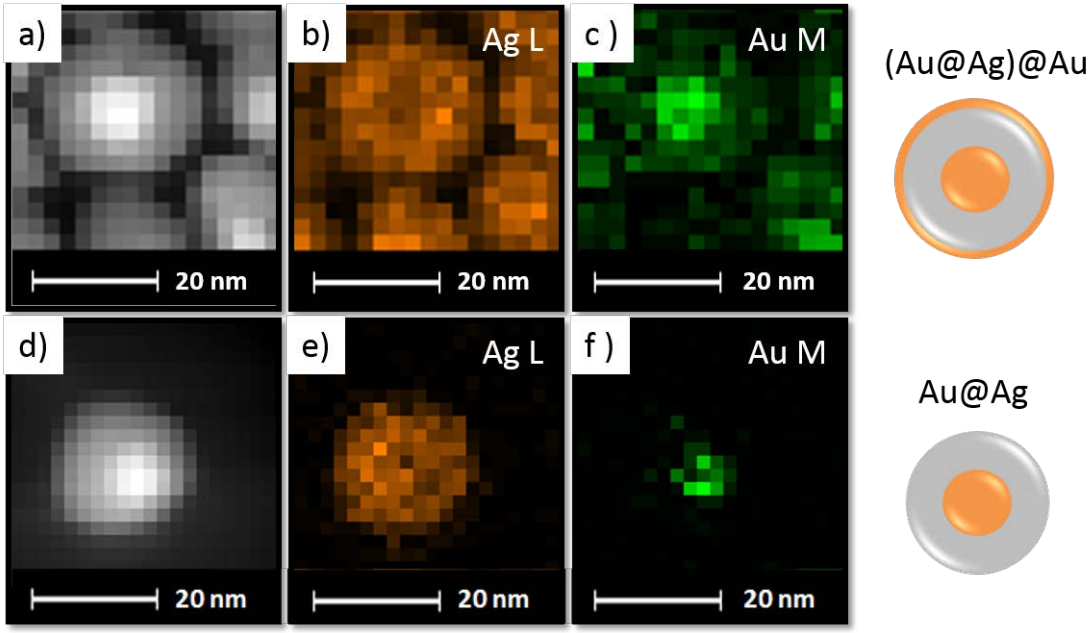

Figure 2. STEM-HAADF image (a) and EDS elemental mapping for Ag L map (b), Au M map (c) of (Au@Ag)@Au NPs. The below images are for Au@Ag NPs with STEM-HAADF image (d) and EDS elemental mapping for Ag L map (e), Au M map (f).

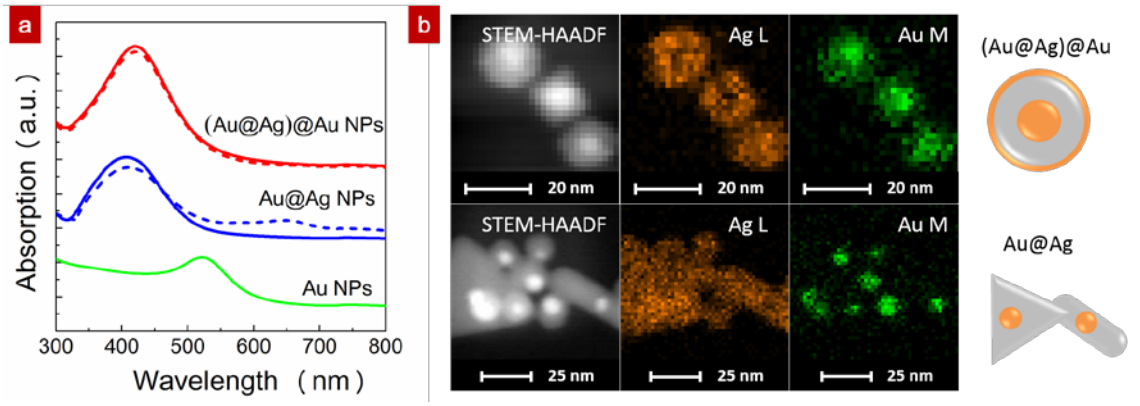

Figure 3. (a) Absorption spectrum of colloidal (Au@Ag)@Au NPs, Au@Ag NPs and Au NPs, where solid lines are as prepared NPs and broken lines indicats after exposure in Xe lamp equipped with Y-44 cut-off filter (λ>440 nm, intensity = 30 mW/cm^2) for 72 hours. (b) STEM-HAADF and EDS elemental mapping images between (Au@Ag)@Au NPs (top) and Au@Ag NPs (bottom) after exposure in Xe lamp for 72 hours (λ>440 nm, intensity = 30 mW/cm^2).

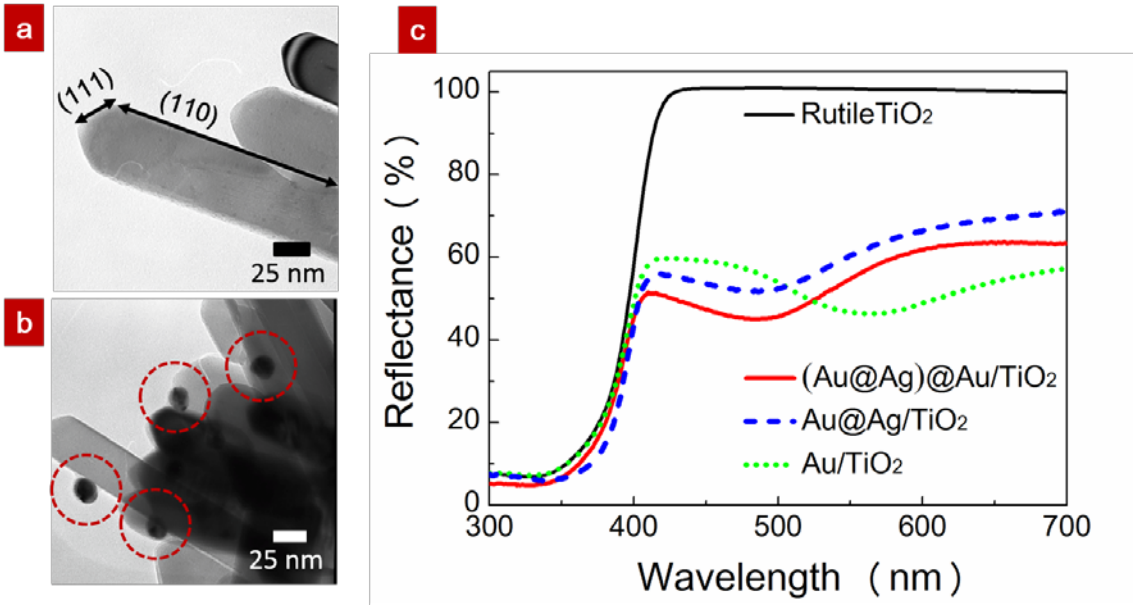

Figure 4. (a) TEM photograph of rutile TiO_2 and (b) (Au@Ag)Au NPs loaded rutile TiO_2 (bottom). (c) Diffuse reflection spectrum of 0.75 w% (Au@Ag)@Au/TiO_2, 0.75 w% Au@Ag/TiO_2, 0.75 w% Au/TiO_2, and bare rutile TiO_2.

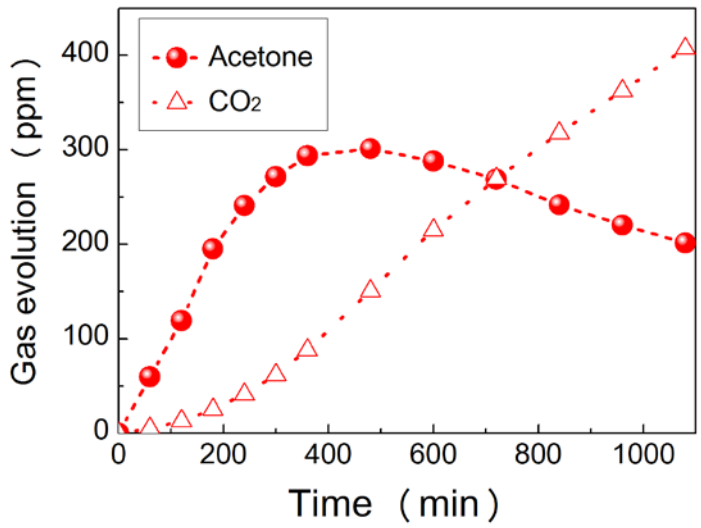

Figure 5. Time course of acetone (solid circle) and CO_2 (open triangle) evolution of 2-propanol decomposition over 0.75 wt% (Au@Ag)Au/TiO_2 under irradiation of Xe lamp equipped with Y-44 cut-off filter (λ>440 nm, intensity = 30 mW/cm^2)

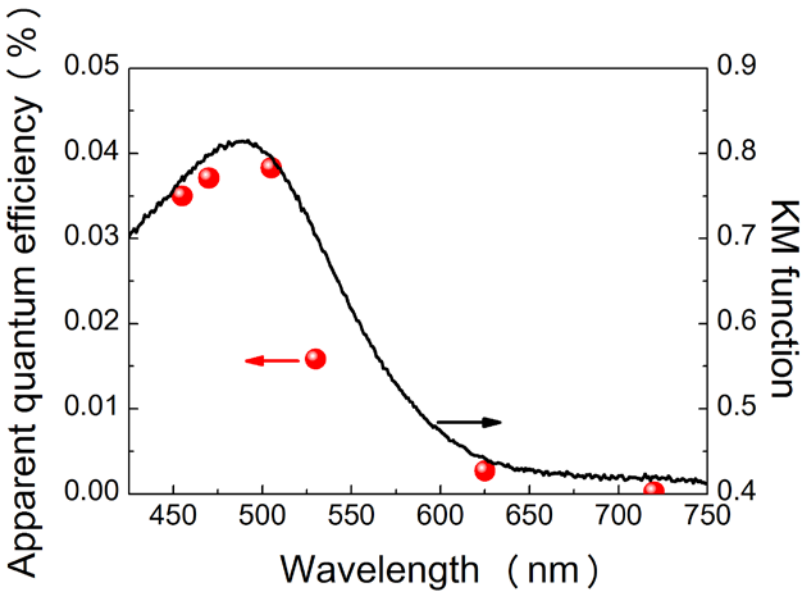

Figure 6. Action spectrum (solid circle) of acetone evolution of 2-propanol decomposition over 0.75 wt% (Au@Ag)Au/TiO_2 (left axis) and Kubelka-Munk function (solid line) of 0.75 wt% (Au@Ag)Au/TiO_2 (right axis).

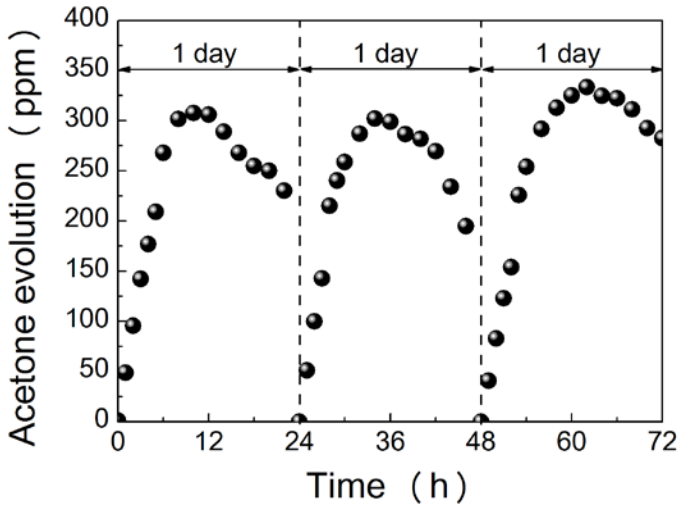

Figure 7. Time course of acetone evolution of 2-propanol decomposition over the 0.75 wt% (Au@Ag)Au/TiO_2 (solid circle) under visible light irradiation for 24 h (Xe lamp, λ>440 nm) which measured up to 3 cycles. After 24 and 48 h irradiation, residual gas was evacuated and additional 2-propanol (500 ppm) was injected and irradiated again.

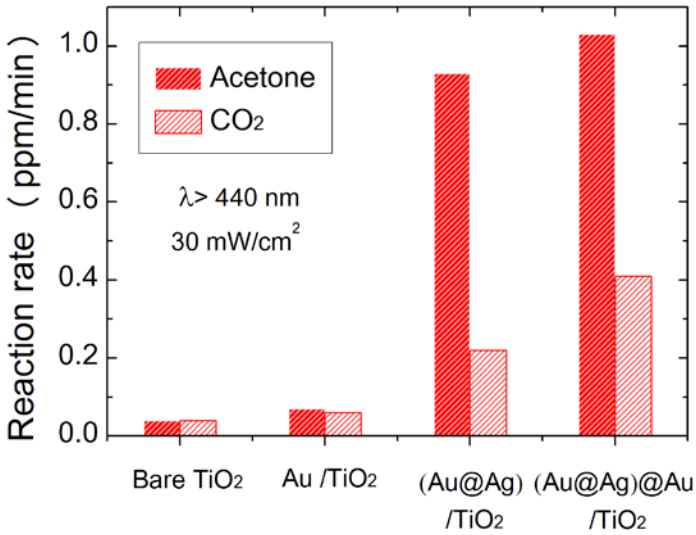

Figure 8. Acetone and CO_2 evolution rates of 2-propanol decomposition over the 0.75 wt% (Au@Ag)Au/TiO_2 under visible light irradiation (Xe lamp, λ>440 nm).

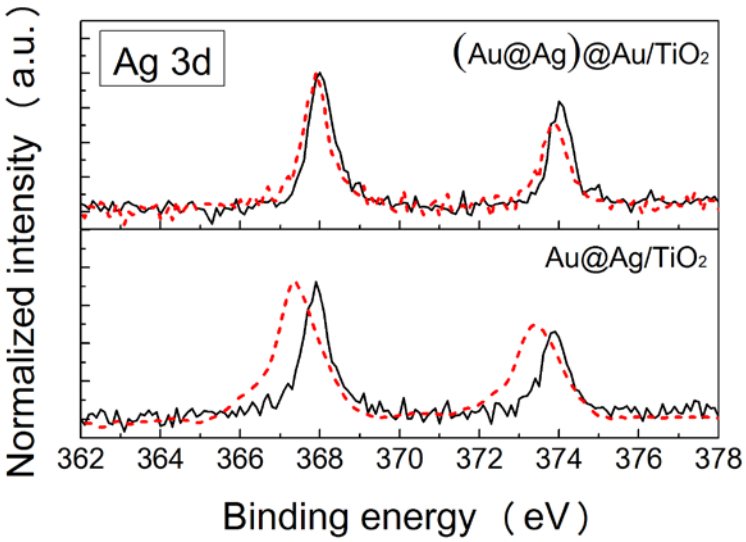

Figure 9. XPS spectra of Ag *3d* of (Au@Ag)@Au/TiO_2 and Au@Ag/TiO_2 before (solid lines) and after (broken lines) photocatalytic activity tests for decomposition of 2-propanol.

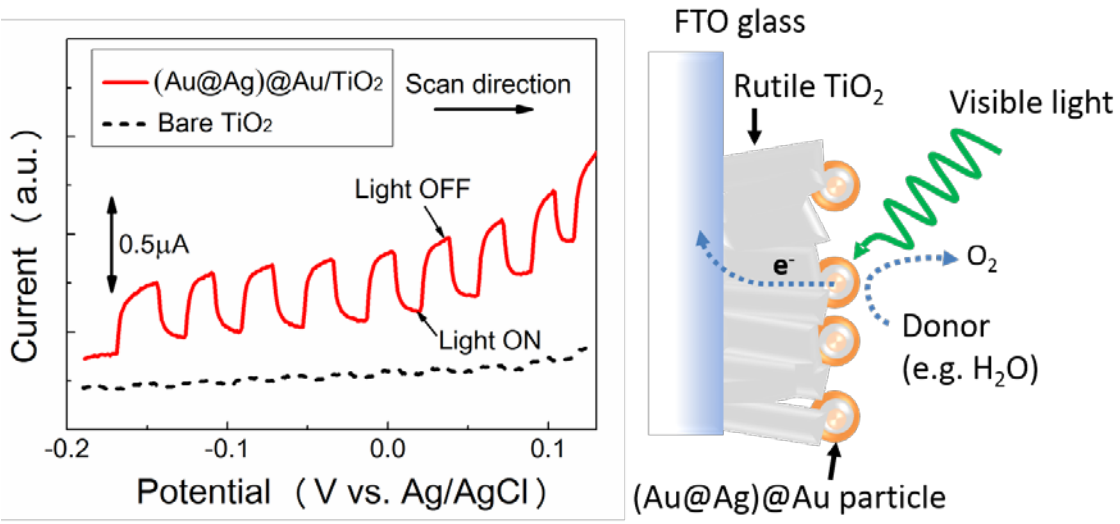

Figure 10. Linear sweep voltammetry of (Au@Ag)@Au/TiO_2 and bare TiO_2 electrode under "chopped" Xe lamp irradiation (λ>440 nm). The electrolyte is non-bubbled aqueous NaOH solution (pH=14). Right figure is expected working mechanism of anodic photocurrent from (Au@Ag)Au/TiO_2 electrode under visible light irradiation.

REFERENCES

(1) Fujishima, A; Honda, K. Electrochemical Photolysis of Water at a Semiconductor Electrode *Nature* **1972**, 238, 37–38.

(2) Hoffmann, M. R; Martin, S. T; Choi, W; Bahnemann D. W. Environmental Applications of Semiconductor Photocatalysis *Chem. Rev.* **1995**, 95, 69–96.

(3) Hashimoto, K; Irie, H; Fujishima, A. TiO_2 Photocatalysis: A Historical Overview and Future Prospects *Jpn. J. Appl. Phys.* **2005**, 12, 8269–8285.

(4) Nakata, K; Fujishima, A. TiO_2 photocatalysis: Design and applications *J. Photochem. Photobiol. C* **2012**, 13, 169–189.

(5) Habisreutinger, S. N.; Schmidt-Mende, L.; Stolarczyk, J. K. Photocatalytic Reduction of CO_2 on TiO_2 and Other Semiconductors. *Angew. Chem., Int. Ed.* **2013**, 52, 7372– 7408.

(6) Kho, Y. K; Iwase, A; Teoh, W. Y; Madler, L; Kudo, A; Ama, R. Photocatalytic H_2 Evolution over TiO_2 Nanoparticles. The Synergistic Effect of Anatase and Rutile *J. Phys. Chem. C* **2010**, 114, 2821–2829.

(7) Ohno, T; Akiyoshi, M; Umebayashi, T; Asai, K; Mitsui, T; Matsumura. M. Preparation of S-doped TiO_2 Photocatalysts and Their Photocatalytic Activities under Visible Light *Appl. Catalysis. A* **2004**, 265, 115–121.

(8) O'regan, B; Grätzel, M. A Low-Cost, High-Efficiency Solar Cell Based on Dye-Sensitized Colloidal TiO_2 Films *Nature* **1991**, 353, 737–740.

(9) Asahi, R; Morikawa, T; Ohwaki, T; Aoki, K; Taga, Y; Visible-Light Photocatalysis in Nitrogen-Doped Titanium Oxides *Science* **2001**, 293, 269–271.

(10) Grätzel, M. Conversion of Sunlight to Electric Power by Nanocrystalline Dye-Sensitized Solar Cells *J. Photochem. Photobiol. A* **2004**, 164, 3–14.

(11) Choi, W; Termin, A; Hoffmann, M. R. The Role of Metal Ion Dopants in Quantum-Sized TiO_2: Correlation between Photoreactivity and Charge Carrier Recombination Dynamics *J. Phys. Chem.* **1994**, 98, 13669–13679.

(12) Wu, T; Liu, G; Zhao, J. Photoassisted Degradation of Dye Pollutants. V. Self-Photosensitized Oxidative Transformation of Rhodamine B under Visible Light Irradiation in Aqueous TiO_2 Dispersions *J. Phys. Chem. B* **1998**, 102, 5845–5851.

(13) Zhao, Y; Swierk, J. R; Megiatto Jr, J. D; Sherman, B; Youngblood, W. J; Qin, D; Lentz, D. M; Moore, A. L; Moore, T. A; Gust, D; Mallouk, T. E. Improving the Efficiency of Water Splitting in Dye-Sensitized Solar Cells by Using a Biomimetic Electron Transfer Mediator *Proc. Natl. Acad. Sci. USA.* **2012**, 109, 15612–15616.

(14) Tian, Y; Tatsuma, T. Mechanisms and Applications of Plasmon-Induced Charge Separation at TiO_2 Films Loaded with Gold Nanoparticles *J. Am. Chem. Soc.* **2005**, 127, 7632–7637.

(15) Kowalska, E; Mahaney O. O. P; Abe R; Ohtani B. Visible-Light-Induced Photocatalysis through Surface Plasmon Excitation of Gold on Titania Surfaces. *Phys. Chem. Chem. Phys.* **2010**, 12, 2344–2355.

(16) Furube, A; Du, L; Hara, K; Katoh, R; Tachiya, M. Ultrafast Plasmon-Induced Electron Transfer from Gold Nanodots into TiO_2 Nanoparticles *J. Am. Chem. Soc.* **2007**, 129, 14852–14853.

(17) Kimura, K; Naya, S; Jin-nouchi, Y; Tada, H; TiO_2 Crystal Form-Dependence of the Au/TiO_2 Plasmon Photocatalyst's Activity. *J. Phys. Chem. C* **2012**, 116, 7111–7117.

(18) Tanaka, A; Sakaguchi, S; Hashimoto, K; Kominami, H. Preparation of Au/TiO_2 with Metal Cocatalysts Exhibiting Strong Surface Plasmon Resonance Effective for

Photoinduced Hydrogen Formation under Irradiation of Visible Light. *ACS Catal.* **2013**, 3, 79–85.

(19) Pincella, F; Isozaki, K; Miki, K. A Visible Light-Driven Plasmonic Photocatalyst. *Light: Science & Applications* **2014**, 3, 1–5.

(20) Tian, Y; Tatsuma, T. Plasmon-Induced Photoelectrochemistry at Metal Nanoparticles Supported on Nanoporous TiO_2. *Chem. Comm.* **2004**, 1810–1811.

(21) Romanyuk, A; Oelhafen. P. Formation and Electronic Structure of TiO_2–Ag Interface Sol. Energy Mater. Sol. Cells 91 (2007) 1051–1054

(22) Yin, Y; Li, Z. Y; Zhong, Z; Gates, B; Xia, Y; Venkateswaranc, S. Synthesis and Characterization of Stable Aqueous Dispersions of Silver Nanoparticles through the Tollens Process *J. Mater. Chem.*, **2002**, 12, 522–527.

(23) Tanabe, I; Tatsuma, T. Plasmonic Manipulation of Color and Morphology of Single Silver Nanospheres *Nano lett.* **2012**, 12, 5418–5421.

(24) Anh, D. T. N; Singh, P; Shankar, C; Mott, D; Maenosono, S. Charge-Transfer-Induced Suppression of Galvanic Replacement and Synthesis of (Au@Ag)@Au Double Shell Nanoparticles for Highly Uniform, Robust and Sensitive Bioprobes *Appl. Phys. Lett.* **2011**, 99, 073107-1–073107-3.

(25) Nishimura, S; Dao, A. T. N; Mott, D; Ebitani, K; Maenosono, S. X-ray Absorption Near-Edge Structure and X-ray Photoelectron Spectroscopy Studies of Interfacial Charge Transfer in Gold-Silver-Gold Double-Shell Nanoparticles *J. Phys. Chem. C* **2012**, 116, 4511−4516.

(26) Bae, K; Ohno, T. Exposed Crystal Surface-Controlled Rutile TiO_2 Nanorods Prepared by Hydrothermal Treatment in the Presence of Poly(vinyl pyrrolidone) *Appl. Catal. B* **2009**, 91, 634−639.

(27) Jin, R; Cao, Y. W; Mirkin, C. A; Kelly, K. L; Schatz, G. C; Zheng, J. G. Photoinduced Conversion of Silver Nanospheres to Nanoprisms *Science* **2001**, 294, 1901−1903.

(28) Wu, X; Redmond, P. L; Liu, H; Chen, Y; Steigerwald, M; Brus, L. Ultrafast Photovoltage Mechanism for Room Light Conversion of Citrate Stabilized Silver Nanocrystal Seeds to Large Nanoprisms *J. Am. Chem. Soc.* **2008**, 130, 9500−9506.

(29) Kakiuchi, K; Hosono, E; Imai, H; Kimura, T; Fujihara, S. {1 1 1}-Faceting of Low-Temperature Processed Rutile TiO_2 Rods *J. Cryst. Growth* **2006**, 293, 541−545.

(30) Ohko, Y; Hashimoto, K; Fujishima, A. Kinetics of Photocatalytic Reactions under Extremely Low-Intensity UV Illumination on Titanium Dioxide Thin Films *J. Phys. Chem. A* **1997**, 101, 8057−8062.

(31) Yamashita, H; Honda, M; Harada, M; Ichihashi, Y; Anpo, M. Preparation of Titanium Oxide Photocatalysts Anchored on Porous Silica Glass by a Metal Ion-Implantation Method and Their Photocatalytic Reactivities for the Degradation of 2-Propanol Diluted in Water *J. Phys. Chem. B* **1998**, 102, 10707−10711.

(32) Irie, H; Miura, S; Kamiya, K; Hashimoto, K. Efficient Visible Light-Sensitive Photocatalysts: Grafting Cu(II) ions onto TiO_2 and WO_3 Photocatalysts *Chem. Phys. Lett.* **2008**, 457, 202−205.

(33) Hoflund, G. B; Hazos, Z. F. Surface Characterization Study of Ag, AgO, and Ag_2O Using X-ray Photoelectron Spectroscopy and Electron Energy-Loss Spectroscopy *Phys. Rev. B* **2000**, 62, 126−133.

(34) Erol, M; Han, Y; Stanley, S. K; Stafford, C. M; Du, H; Sukhishvili, S. SERS Not to be Taken for Granted in the Presence of Oxygen *J. Am. Chem. Soc.* **2008**, 130, 9500−9506.